International Journal of Bifurcation and Chaos, Vol. 9, No. 3 (1999) 561–570

VIBRATION OF EXTERNALLY-FORCED FROUDE PENDULUM

GRZEGORZ LITAK, GRZEGORZ SPUZ-SZPOS,
KAZIMIERZ SZABELSKI and JERZY WARMIŃSKI
Department of Mechanics, Technical University of Lublin,
Nadbystrzycka 36, Lublin 20–618, Poland

Received January 6, 1997; Revised September 7, 1997

Motion of self-excited Froude pendulum under external forcing were analyzed. Differential equation of motion includes the nonlinear damping term of Rayleigh's type. Using multiple time scale method and Lyapunov theory, vibrations, synchronization and stability of the system were examined. Chaotic motion was analyzed here by means of Lyapunov exponent and Melnikov approach.

1. Introduction

Froude pendulum is an example of self-excited system [Minorski, 1962; Moon, 1987; Litak *et al.*, 1994, 1996]. The system consists of pendulum suspended on a rotating shaft (Fig. 1). Friction between the shaft and the suspension causes the self-excitation of the pendulum.

Vibrations of pendulum subjected to external excitation can be described by the following differential equation:

$$\ddot{\varphi} - (\tilde{\alpha} - \tilde{\beta}\dot{\varphi}^2)\dot{\varphi} + \tilde{\delta} \sin \varphi = \tilde{B} \cos \omega t\,, \qquad (1)$$

where $\tilde{\alpha}$, $\tilde{\beta}$ denote nonlinear Rayleigh damping term coefficients, $\tilde{B}$ excitation amplitude, ω excitation frequency, $\tilde{\delta}$ is the typical pendulum nonlinear term coefficient dependent on the geometry of the system.

Such a system is described by two characteristic frequencies: the frequency of self-excited vibration and the external excitation frequency. For exciting force amplitude $\tilde{B}$ equal to zero vibration with the same frequency as for a self-excited system appears. For $\tilde{B} > 0$, according to the parameters of the system, it is likely to occur as two cases of regular solutions: mono-frequency solution or quasiperiodic solution with a modulated amplitude. In such a system, besides regular solutions, chaotic solutions may also appear [Litak *et al.*, 1994, 1996]. The aim of this note is to provide general discussion on the vibration of self-excited systems with external forcing by analyzing the example Froude pendulum. The article is organized as follows: After a short introduction (in Sec. 1) we analyze vibration in the vicinity of fundamental external resonance (Sec. 2) and obtain analytic forms of the solution. These results are used in Sec. 3 where we provide an analysis of the stability solution by applying Lyapunov theory and we proceed with the discussion on the synchronization phenomenon. The comparison between analytic and numerical simulation results is also given. Section 4 is devoted to the Melnikov analysis of Froude pendulum motion. The principal result of this section is the analytic form of critical amplitude $\tilde{B}_C$ above which chaotic solution exists. Numerical calculations by means of Lyapunov exponent method confirm these analytic results for a chosen set of examined system parameters. Section 5 concerns the numerical exploration of chaotic motion of the examined system. We then investigate chaotic motion using different methods. Lyapunov exponent criterion is applied to find regions of

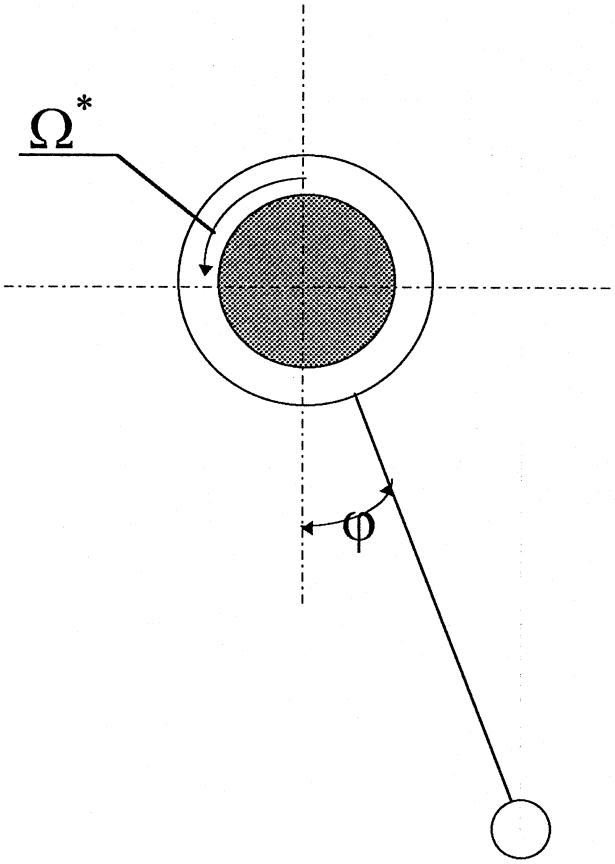

Fig. 1. Frude pendulum, ω^* — angular velocity, φ — vibration angle.

parameters indicating chaotic behavior. Some examples of Poincare maps, time histories, basins of attraction and a power spectrum are plotted to illustrate the types and the evolutions of attractors. In Sec. 6 we end up with summary and conclusions.

2. Solution in the Vicinity of Fundamental External Resonance

Let us examine small vibrations around $\varphi = 0$, expanding in Taylor's series up to the third-order terms $\sin(\varphi) \approx \varphi - \tilde{\gamma}\varphi^3$, where $\tilde{\gamma} = (1/6)\tilde{\delta}$ yields the following equation:

$$\ddot{\varphi} - (\alpha - \tilde{\beta}\dot{\varphi}^2)\dot{\varphi} + (\tilde{\delta} - \tilde{\gamma}\varphi^2)\varphi = \tilde{B}\cos\omega t\,. \quad (2)$$

For the fundamental external resonance we can write:

$$\omega^2 \approx \tilde{\delta} + \varepsilon\sigma\,. \quad (3)$$

Introducing the small parameter $\varepsilon \ll 1$ into Eq. (2) and using the approximation (3) we get for $\tilde{\delta} = 1$:

$$\ddot{\varphi} + \omega^2\varphi = \varepsilon[\sigma\varphi + (\alpha - \beta\dot{\varphi}^2)\dot{\varphi} + \gamma\varphi^2)\varphi + B\cos\omega t]\,, \quad (4)$$

where $\tilde{\beta} = \varepsilon\beta$, $\tilde{B} = \varepsilon B$, $\tilde{\alpha} = \varepsilon\alpha$, $\tilde{\gamma} = \varepsilon\gamma$.

Using the standard multiple-time-scale procedure [Nayfeh & Sanchez, 1989] we decouple time derivatives into:

$$\frac{d}{dt} = D_0 + \varepsilon D_1 + \varepsilon^2 D_2 + \cdots\,,$$
$$\frac{d^2}{dt^2} = D_0^2 + 2\varepsilon D_0 D_1 + \varepsilon^2(2D_0 D_2 + D_1^2) + \cdots\,, \quad (5)$$

where $D_n = \partial/\partial T_n$ and $T_n = \varepsilon^n t$.

We evaluate the general form of the solution

$$\varphi = \varphi(T_0, T_1, \ldots; \varepsilon) \quad (6)$$

to the first-order approximation of type:

$$\varphi(t) \approx a\cos(\omega t + \psi)\,. \quad (7)$$

After some algebra we have found the following equations for a and ψ:

$$\dot{a} = \varepsilon\left(\frac{\alpha}{2}a - \frac{3}{8}\beta a^3 - \frac{B}{2\omega}\sin\psi\right) \quad (8)$$

$$a\dot{\psi} = \varepsilon\left(-\frac{\sigma_1}{2\omega}a - \frac{3\gamma}{8\omega}a^3 - \frac{B}{2\omega}\cos\psi\right)\,. \quad (9)$$

The second-order approximation reads:

$$\varphi(t) = a\cos(\omega t + \psi) - \varepsilon\left(\frac{\gamma a^3}{32\omega^2} - \frac{3\mathrm{i}\beta a^3}{32\omega}\right)\cos(3\omega t + 3\psi)\,, \quad (10)$$

where a and ψ have to fulfil the equations:

$$\dot{a} = \varepsilon\frac{\alpha}{2}a - \varepsilon\frac{3}{8}\beta a^3 + \varepsilon^2\frac{3\alpha\gamma}{16\omega^2}a^3 - \left(\varepsilon\frac{B}{2\omega} + \varepsilon^2\frac{\sigma B}{8\omega^3} + \varepsilon^2\frac{9\gamma B}{32\omega^3}a^2\right)\sin\psi + \varepsilon^2\left(\frac{3\beta B a^2}{32\omega^2} - \frac{\alpha B}{8\omega^2}\right)\cos\psi\,, \quad (11)$$

$$a\dot{\psi} = -\left(\varepsilon\frac{\sigma}{2\omega} + \varepsilon^{\frac{\alpha^2}{8\omega}} + \varepsilon^2\frac{\sigma^2}{8\omega^3}\right)a - \left(\varepsilon\frac{3\gamma}{8\omega} + \varepsilon^2\frac{\gamma\sigma}{16\omega^3} - \varepsilon^2\frac{3\alpha\beta}{8\omega}\right)a^3 - \varepsilon^2\left(\frac{15\gamma^2}{256\omega^3} + \frac{63\beta^2}{256\omega}\right)a^5$$
$$-\left(\varepsilon\frac{B}{2\omega} + \varepsilon^2\frac{\sigma B}{8\omega^3} + \varepsilon^2\frac{3\gamma B}{32\omega^3}a^2\right)\cos\,\psi - \varepsilon^2\left(\frac{9\beta B}{32\omega^2}a^2 - \frac{\alpha B}{8\omega^2}\right)\sin\,\psi\,. \tag{12}$$

Equations (7)–(12) are the principal result of that section. They will be used in the analysis of the system stability and synchronization of the pendulum motion with the external forcing in the next section.

3. The Periodic Solution Stability Analysis

The stability solution analysis was carried out by using approximate differential equations of the first order [Eqs. (8) and (9)] in a shortened form:

$$\frac{da}{dt} = F_1(a,\,\psi), \qquad a\frac{d\psi}{dt} = F_2(a,\,\psi)\,. \tag{13}$$

Putting disturbances into Eqs. (13)

$$\delta_1 = \tilde{a}(t) - a(t), \qquad \delta_2 = \tilde{\psi}(t) - \psi(t)\,, \tag{14}$$

where $\tilde{a}(t)$ and $\tilde{\psi}(t)$ are the solutions corresponding to the insignificantly-changed initial conditions, from which one obtains the differential equations of disturbed motion. After subtraction of the undisturbed motion Eqs. (8) and (9) from the equations of disturbed motion one gets other linearized differential equation for variations δ_1 and δ_2:

$$\begin{aligned}\frac{d\delta_1}{dt} &= \left(\frac{\partial F_1}{\partial a}\right)_0\delta_1 + \left(\frac{\partial F_1}{\partial \psi}\right)_0\delta_2\,,\\ \frac{d\delta_2}{dt} &= \left(\frac{\partial F_2}{\partial a}\right)_0\delta_1 + \left(\frac{\partial F_2}{\partial \psi}\right)_0\delta_2\,,\end{aligned} \tag{15}$$

where

$$\begin{aligned}\frac{\partial F_1}{\partial a} &= \left(\frac{1}{2}\alpha - \frac{9}{8}\beta a^2\right)\varepsilon\,,\\ \frac{\partial F_1}{\partial \psi} &= -\frac{1}{2}\frac{\beta}{\omega}\cos\,\psi\varepsilon\,,\\ \frac{\partial F_2}{\partial a} &= \left(-\frac{1}{2}\frac{\sigma}{\omega} - \frac{3}{4}\gamma\frac{a^2}{\omega}\right)\varepsilon\,,\\ \frac{\partial F_2}{\partial \psi} &= \frac{1}{2}\frac{B}{\omega}\sin\,\psi\varepsilon\,.\end{aligned} \tag{16}$$

The subscript "0" indicates that the derivative values are taken in the equilibrium state. For assumed solutions of type:

$$\delta_1 = C_1\mathrm{e}^{\rho t}, \qquad \delta_2 = C_2\mathrm{e}^{\rho t}\,, \tag{17}$$

where C_1 and C_2 are arbitrary constants.

When substituting solutions [Eqs. (17)] in Eq. (15) yields the following characteristic equation for the variable ρ:

$$\mathrm{Det}\begin{bmatrix}\left(\frac{\partial F_1}{\partial a}\right)_0 - \rho & \left(\frac{\partial F_1}{\partial \psi}\right)_0\\ \left(\frac{\partial F_2}{\partial a}\right)_0 & \left(\frac{\partial F_2}{\partial \psi}\right)_0 - \rho\end{bmatrix} = 0\,. \tag{18}$$

The stability condition in the Lyapunov formulation [Szabelski & Warmiński, 1995] requires solution with negative real terms for ρ of the above characteristic equation [Eq. (18)]. To proceed this schema one must calculate values of ρ for each value of ω. The results of such calculations are presented in Table 1. Figure 2 shows a plot of the vibration amplitude versus the frequency of external excitation ω. It has been obtained as a result of analytical research (AR) in the first-order approximation of perturbation procedure [Eqs. (8) and (9)]. Types of system stability for different ω are also marked in this picture according to Table 1. Comparative points obtained during numerical simulation by means of Runge–Kutta–Gill (RKG) algorithm [Eq. (1)] were also marked.

Parameters used in the investigations are the following: $\tilde{\alpha} = 0.035$, $\tilde{\beta} = 0.1$, $\tilde{B} = 0.1$, $\tilde{\gamma} = 1/6$, $\varepsilon = 0.1$. Beats are marked here by vertical lines terminated by circles on the ends which correspond

Table 1. Vibration stability.

ω	Type of Singularity
0.800–0.878	unstable focus
0.878–0.893	stable focus
0.888–0.892	saddle point
0.876–0.900	stable node
0.900–1.078	stable focus
1.078–1.150	unstable focus

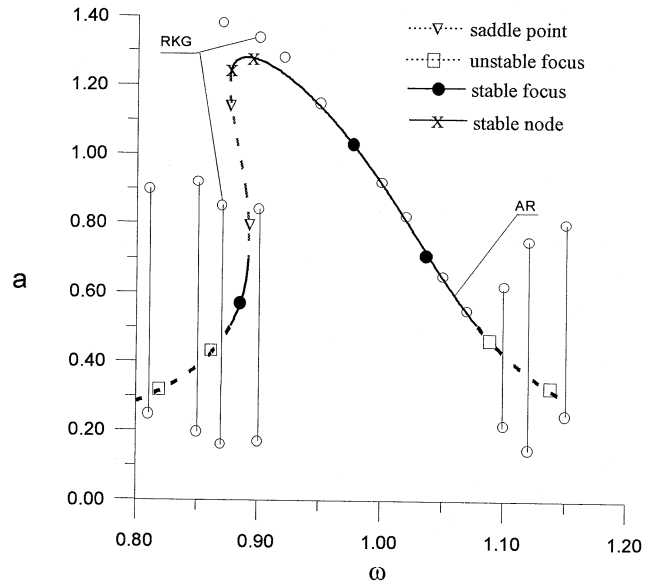

Fig. 2. Vibration amplitude **a** versus excitation frequency ω. RKG denote the numerical results and AR the analytic ones.

to the maximal and minimal values of vibration amplitudes (Fig. 2). In Fig. 3 we present examples of time histories. The synchronized mono-frequency vibration is shown in Fig. 3(b) ($\omega = 0.95$). Outside the synchronization area beats, i.e. quasiperiodic vibrations occur. The typical time history in this region is presented in Fig. 3(a), where ω was chosen to be equal to 0.85.

4. Transition to Chaos, Melnikov Analysis

Melnikov approach enables us to find critical values of system parameters for which chaotic solutions appear. This method is based on analyzing Smale horseshoe schemes on phase plane. Starting our examination from Poincaré maps of Hamiltonian system we investigate quasiperiodic orbits which begin and finish at saddle points φ_i^0, v_i^0, ($v = \dot{\varphi}$). These orbits are called homoclinic

$$\lim_{t\to-\infty}(\varphi_1, v_1) = \lim_{t\to\infty}(\varphi_1, v_1) = (\varphi_0^0, v_0^0) \qquad (19)$$

and heteroclinic

$$\begin{aligned} \lim_{t\to-\infty}(\varphi_1, v_1) &= (\varphi_1^0, v_1^0) \\ \lim_{t\to\infty}(\varphi_1, v_1) &= (\varphi_2^0, v_2^0)\,, \end{aligned} \qquad (20)$$

where $(\varphi_2^0, v_2^0) \neq (\varphi_1^0, v_1^0)$.

In our case of the examined Frude pendulum, the orbits correspond to heteroclinic ones unless we identify points $(\varphi^I, v) = (-\pi, v)$ and $(\varphi^{II}, v) = (\pi, v)$, and arbitrary v on phase plane using cylindrical φ coordinate. Analyzing Hamiltonian heteroclinic orbits we examine stable and unstable manifolds introducing external force and damping as perturbations. Equation (1) (for $\tilde{\delta} = 1$) may be

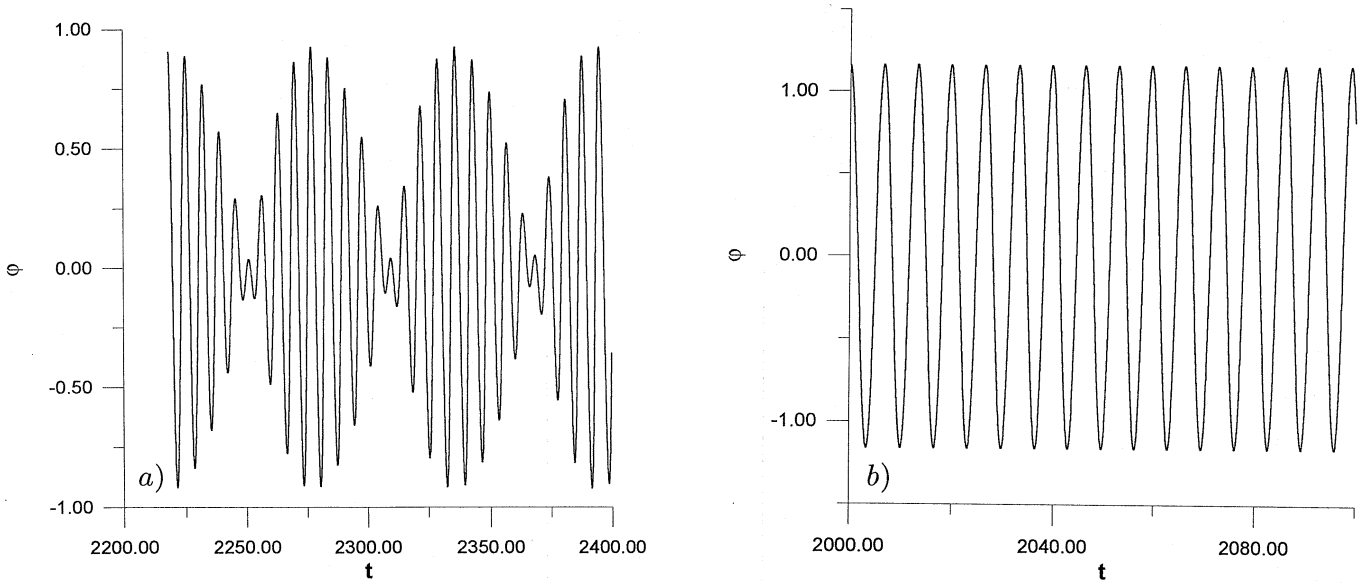

Fig. 3. Time histories for (a) $\omega = 0.85$, (b) $\omega = 0.95$.

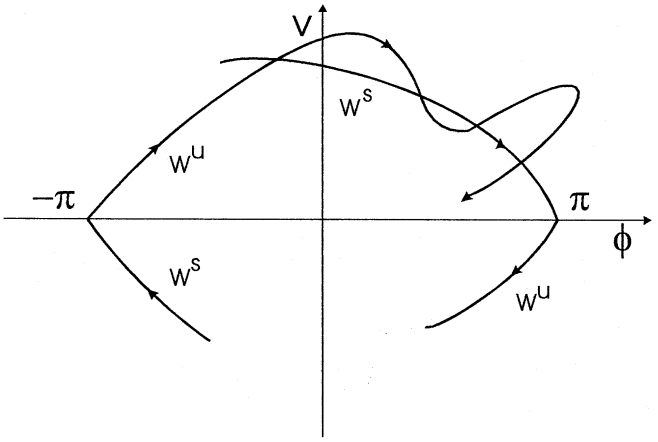

Fig. 4. Stable W^S and unstable W^U manifolds for a damped and excited system.

written as follows:

$$\begin{aligned} \dot{\varphi} &= v \\ \dot{v} &= -\sin\,\varphi + \varepsilon[(\alpha - \beta v^2)v + B\,\cos\,\omega t]\,, \end{aligned} \tag{21}$$

where ε denotes perturbation parameter.

In Fig. 4 stable W^S and unstable W^U manifolds are presented schematically. Intersection points indicate on Smale horseshoes schemes typical for chaotic systems [Moon, 1987].

Nodal value of Melnikov function [Guckenheimer & Holms, 1983; Wiggins, 1988; Salam, 1987] $M(t)$ which determine the distance d between these two manifolds is the criterion of chaotic solution appearance.

$$d = M(t_0) = \int_{-\infty}^{\infty} h(\varphi^*,\, v^*) \wedge g(\varphi^*,\, v^*)dt \tag{22}$$

where differential forms $h = h_1 d\varphi + h_2 dv$ and $g = g_1 d\varphi + g_2 dv$ are defined as the gradient of unperturbed Hamiltonian $H = (1/2)v^2 + (1 - \cos\,\varphi)$ in phase plane and perturbation terms are $g_1 = 0$, $g_2 = (\alpha - \beta v^2)v + B\,\cos(\omega(t - t_0))$, respectively. Stars marked by φ and v (φ^*, v^*) denote that forms h and g are defined on heteroclinic manifolds of the corresponding Hamiltonian system:

$$\begin{aligned} \varphi^* &= \pm 2\tan^{-1}(\sinh t) \\ v^* &= \pm\frac{2}{\cosh t}\,. \end{aligned} \tag{23}$$

After some algebra we find:

$$M(t_0) = 8\alpha - \frac{64}{3}\beta + 2\pi\frac{\cos(\omega t_0)}{\cosh(\omega\pi/2)}B\,. \tag{24}$$

The condition of chaotic solution occurrence [Guckenheimer & Holms, 1983; Wiggins, 1988] has following form

$$\exists t_0 \qquad M(t_0) = 0, \qquad \frac{\partial M(t_0)}{\partial t_0} \neq 0\,. \tag{25}$$

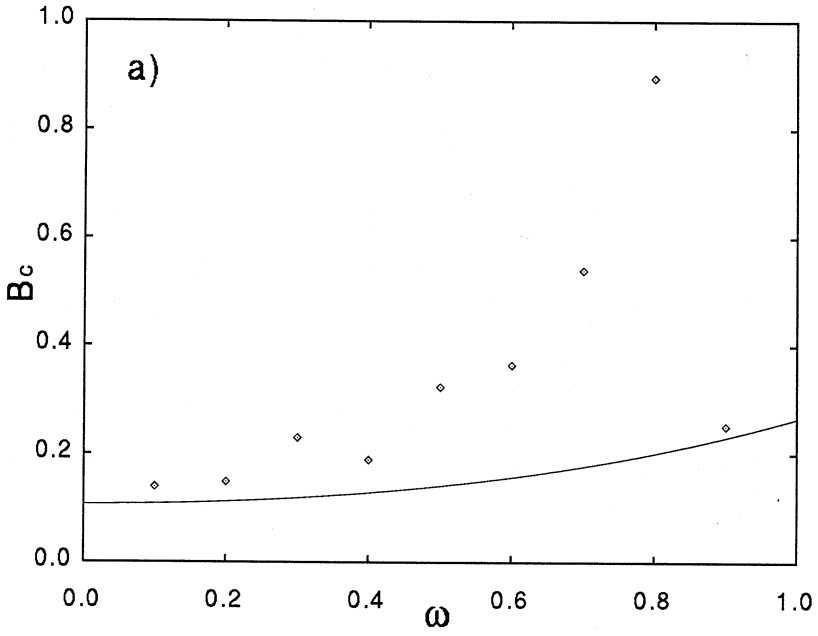

Fig. 5. Critical amplitude $B_C = \tilde{B}_C$ versus excitation frequency ω for (a) $\tilde{\alpha} = 0.35$ and (b) $\tilde{\alpha} = 0.035$. Lines correspond to analytic solution and diamonds to numerical simulations.

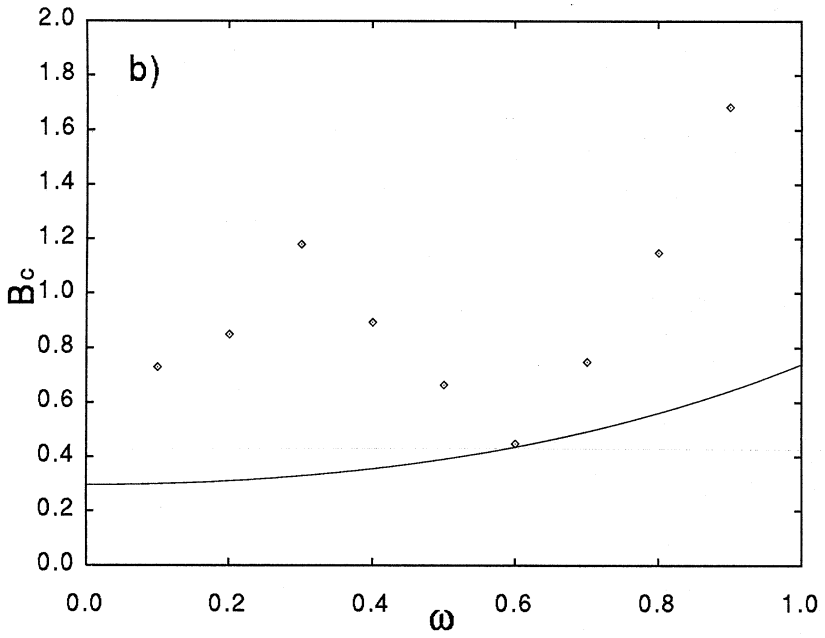

Fig. 5. (*Continued*)

Thus, the critical amplitude of the external forcing, for which condition (16) is fulfilled is shown as follows:

$$\tilde{B}_C = \frac{4}{\pi}\left|\tilde{\alpha} - \frac{8}{3}\tilde{\beta}\right| \cosh\left(\frac{\omega\pi}{2}\right) . \qquad (26)$$

The condition for a simple damped mathematical pendulum with external forcing has similar form. In such a system instead of the factor $|\tilde{\alpha} - (8/3)\tilde{\beta}|$ we write simply $\tilde{\alpha}$.

In Fig. 5 we show critical amplitude $\tilde{B}_C$ as a function of external forcing frequency for two sets of damping coefficient values $\tilde{\alpha} = 0.35$, $\tilde{\beta} = 0.1$ [Fig. 5(a)] and $\tilde{\alpha} = 0.035$, $\tilde{\beta} = 0.1$ [Fig. 5(b)]. For $\tilde{B} > \tilde{B}_C$ solution of the chaotic type may occur while for $\tilde{B} < \tilde{B}_C$ solution should be of the regular type. Comparative points for $\tilde{B}_C$ obtained by numerical simulations by means of Lyapunov exponent method (Sec. 5) are depicted by diamonds. Note that numerical results give usually larger values of critical amplitude $\tilde{B}_C$ than analytic ones [Moon, 1987].

5. Analysis of Chaotic Motion

The most reliable criterion for chaotic deterministic motion is the positive value of the maximal (but nonzero) Lyapunov exponent. Figure 6 presents the results values of Lyapunov exponents λ_1 versus excitation amplitude $\tilde{B}$ calculated by Wolf *et al.*'s algorithm [1988]. For numerical simulations [Eq. (1)], the following parameters: $\tilde{\delta} = 1$, $\omega = 1$, $\tilde{\beta} = 0.1$, $\tilde{\alpha} = 0.35$ [Fig. 6(a)] and $\tilde{\alpha} = 0.035$ [Fig. 6(b)] the initial conditions: $\varphi_0 = 0$, $\dot{\varphi}_0 = 0.5$ have been used.

For intervals around $\tilde{B} \approx 2.5$ chaotic motions of pendulum have been found in both cases ($\tilde{\alpha} = 0.35$, $\tilde{\alpha} = 0.035$). The additional interval around $\tilde{B} \approx 0.45$ for $\tilde{\alpha} = 0.35$ shows the chaotic behavior which is absent in the case of smaller $\tilde{\alpha}$. For four values of the external amplitude $\tilde{B}$: $\tilde{B} = 0.1$, 0.42, 1,2, 2.5, Poincaré maps are presented [Figs. 7(a)–(d)]. Each picture has been obtained using a number of sets of initial conditions. Other parameter values of the system have been chosen as in Fig. 6(a). In calculations points $(-\pi, v)$ and (π, v) (for arbitrary v) have been identified. Starting from small forcing, Fig. 7(a) shows regular quasiperiodic motion. This is connected with the self-excitation of the pendulum. Note that the limit cycles are not connected and form the separate upper and lower branches. They correspond to different initial conditions used in simulations. For a larger forcing amplitude Figs. 7(b) and 7(d) illustrate the strange attractors of pendulum chaotic motion and Fig. 7(c) mono-frequency synchronized motion represented by the singular point.

In Fig. 8, for the same system parameters we present two different bifurcation diagrams according to different initial conditions [corresponding to the upper and lower branches of Poincaré maps in Fig. 7(a)]. Here again $\tilde{B}$ was treated as a

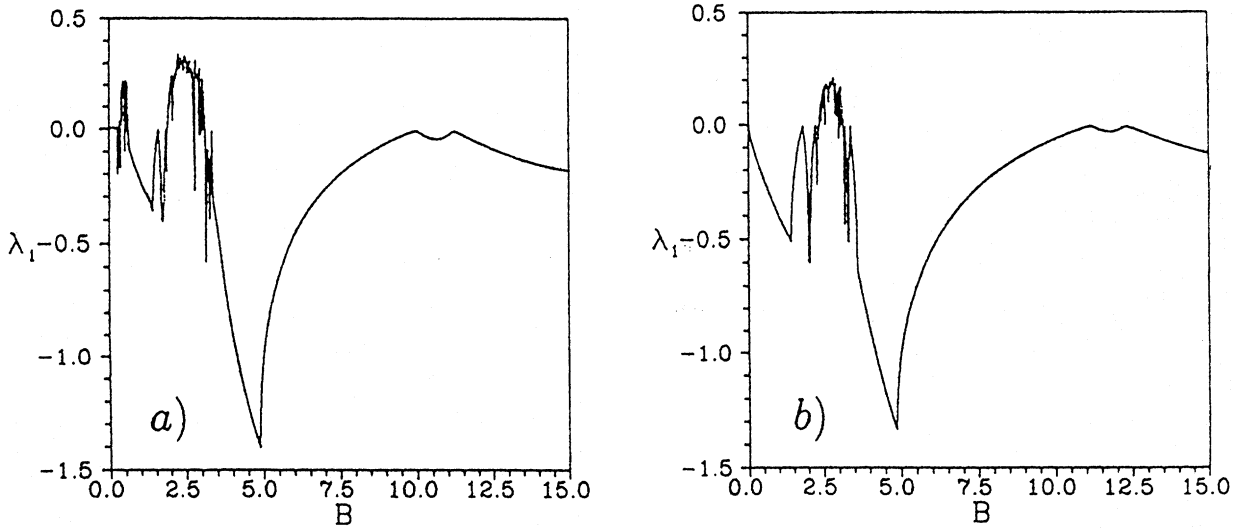

Fig. 6. The maximal Lyapunov exponent λ_1 versus external amplitude $B = \tilde{B}$: $\tilde{\alpha} = 0.35$ [Fig. 6(a)], $\tilde{\alpha} = 0.035$ [Fig. 6(b)].

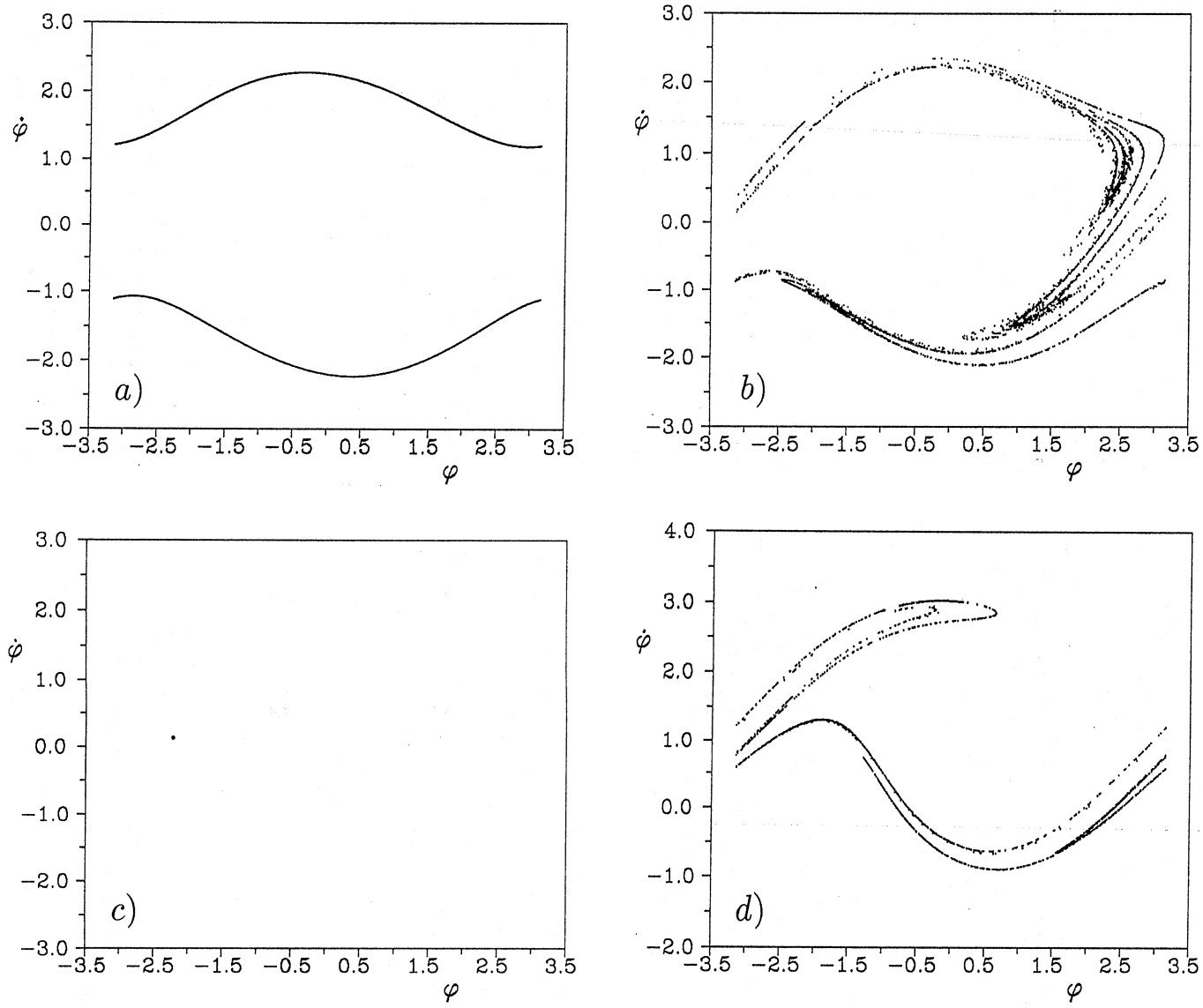

Fig. 7. Poincaré maps. $\tilde{B} = 0.1$, 0.42, 1.2, 2.5 for 7(a)–7(d), respectively.

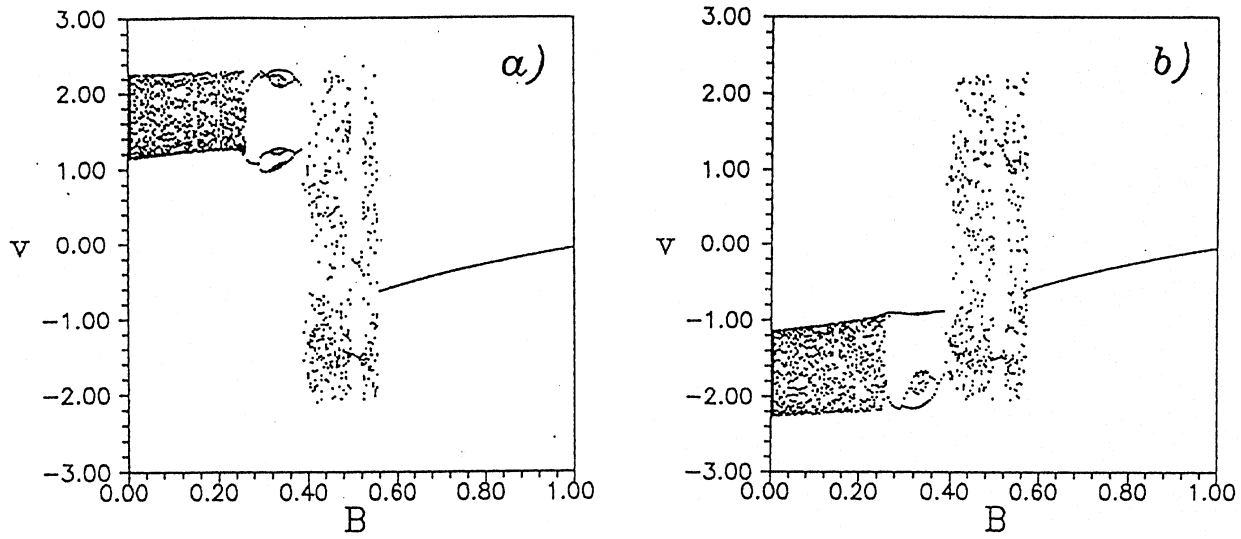

Fig. 8. Bifurcation diagrams for initial conditions: (a) $(\varphi_0,\, v_0) = (0,\, 1.0)$ and (b) $(\varphi_0,\, v_0) = (0,\, 0.5)$.

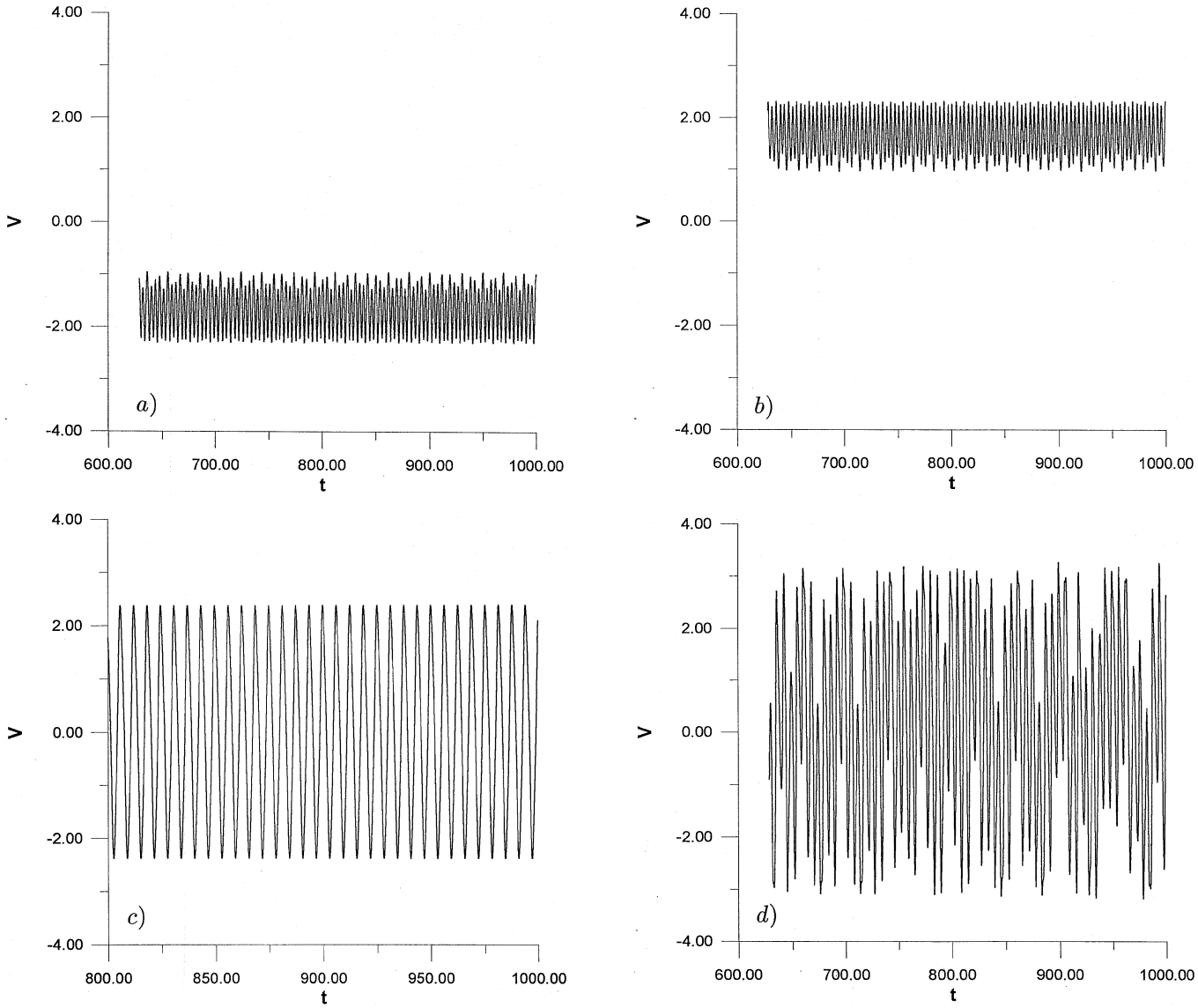

Fig. 9. Time histories for: $\tilde{B} = 0.1$ and the initial conditions (a) $(\varphi_0,\, v_0) = (0,\, 0.5)$, (b) $(\varphi_0,\, v_0) = (0,\, 1.0)$; (c) $\tilde{B} = 1.2$ and (d) $\tilde{B} = 2.5$ for the initial conditions $(\varphi_0,\, v_0) = (0,\, 0.5)$.

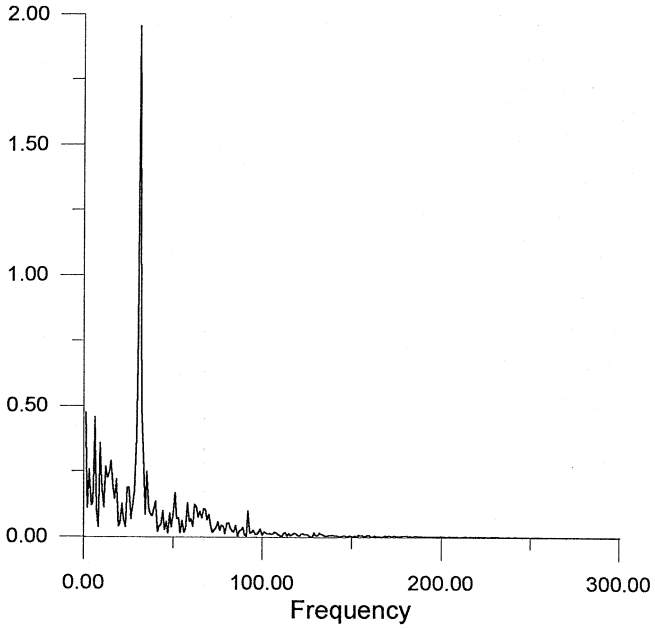

Fig. 10. Power spectrum for $\tilde{B} = 2.5$.

bifurcation parameter. Figure 8(a) corresponds to following initial conditions: $\varphi_0 = 0$, $v_0 = 1.0$ and Fig. 8(b): $\varphi_0 = 0$, $v_0 = 0.5$, respectively. Thus the regular motion of Froude pendulum could be synchronized with external forcing for $\tilde{B} \in [0.23, 0.4]$ and $[0.48, 1.0]$ or quasiperiodic for $\tilde{B} \in [0.0, 0.23]$. This picture also confirms our earlier exploration by Lyapunov exponent [Fig. 6(a)].

For better clarity time histories which correspond to various types of motion have been plotted in Fig. 9. Figures 9(a) and 9(b) show evidently the left and right quasiperiodic rotations. Note that time histories are plotted for velocities $v = \dot{\varphi}$ (Fig. 9) instead of angles φ (Fig. 3). In these pictures one can see oscillations of $\dot{\varphi}$ in time in a narrow region of velocities without the change of sign. On the other hand the periodic motion of pendulum is presented in Fig. 9(c) for $\tilde{B} = 1.2$. Here we recognize the full spectrum of velocities with both signs changing in the periodic way. This means that the motion has been synchronized with external forcing. Applying the same analysis for $\tilde{B} \in [0.23, 0.4]$ (see Fig. 8) we have also checked that in this interval of amplitude $\tilde{B}$, right and left rotations synchronized with the external forcing frequency appeared.

The last time history [Fig. 9(d)] corresponds to the chaotic motion of the pendulum $\tilde{B} = 2.5$. For this value of external amplitude the pendulum shows nonperiodic oscillations. This nonperiodicity is better visible in Fig. 10 where we have plotted the power spectrum for the same system parameters. The broadened interval of frequencies refer here to chaotic motion instead of individual frequencies which always represent a regular motion.

Additionally Fig. 11 presents the basins of attraction for rotational and chaotic motions of the pendulum ($\omega = 1$, $\tilde{\alpha} = 0.35$, $\tilde{\beta} = 0.1$, $\tilde{\delta} = 1$).

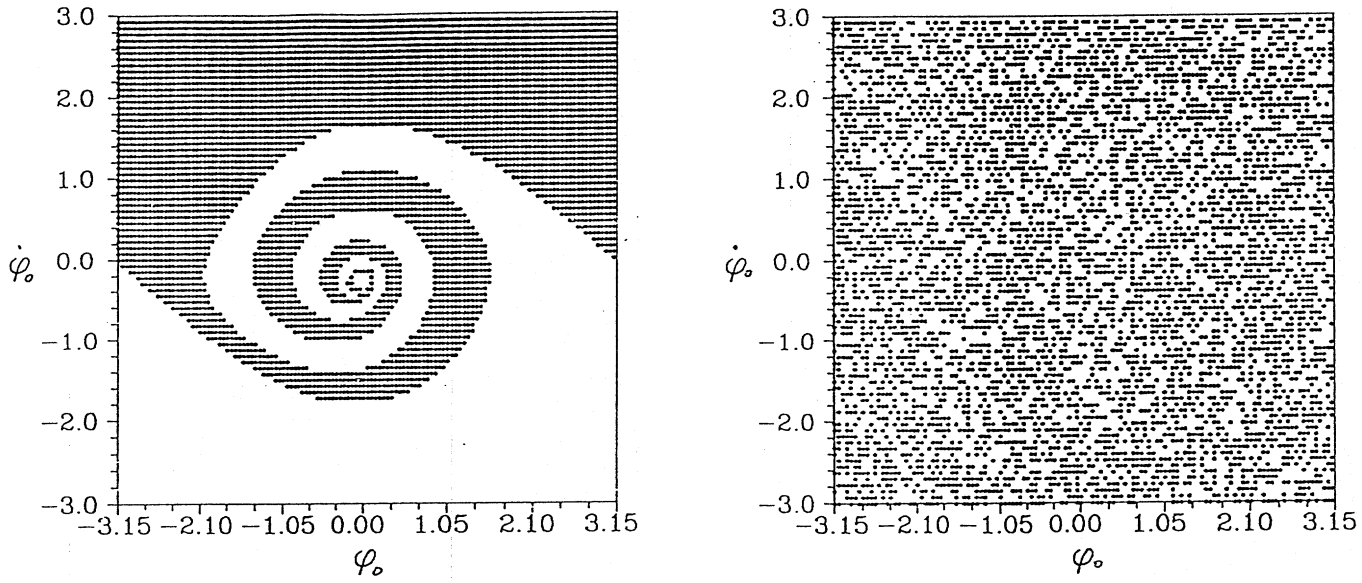

Fig. 11. Basins of attraction for (a) $\tilde{B} = 0.1$ and (b) $\tilde{B} = 2.5$.

In Fig. 11(a) ($\tilde{B} = 0.1$) one can recognize the initial conditions which lead to left (empty space) and right (black points) rotations of the pendulum. They are placed alternately in the phase plane (φ_0, $\dot{\varphi}_0$). The border separating these two regions is well defined. Figure 11(b) corresponds to chaotic motion. In this picture there is no border between two basins of attraction. The picture also has self-similar structures in different scales.

6. Summary and Conclusions

Analytic and numerical investigations were carried out for Froude pendulum. The synchronization region was obtained under certain simplified assumptions and their verification was obtained applying numerical simulation. Chaotic vibrations and quasiperiodic rotation of pendulum was investigated by means of Melnikov criterion and Lyapunov exponent, Poincaré maps and bifurcation diagrams and power spectra for particular parameters of the system.

The structures of strange attractors of Frude pendulum is similar to that of a simple mathematical one [Baker & Gollub, 1990]. However we noticed some differences in scenario for transition to chaos. We found that quasiperiodic vibrations appear outside the synchronization region for small $\tilde{\alpha}$ [Fig. 1(b)] while quasiperiodic rotations appear for large enough $\tilde{\alpha}$ [$\tilde{\alpha} = 0.35$ — Figs. 7(a), 9(a) and 9(b)]. We have shown in Fig. 2(a) that for the region of relatively small external excitation $\tilde{B}$, where quasiperiodic rotations appear, Lyapunov exponent λ_1 has nodal value.

Thus in the self-excited Froude pendulum, where the additional characteristic self-excitation frequency is present, we have found that the type of regular motion is controlled by Rayleigh damping coefficients i.e. for small $\tilde{\alpha}$ coefficients (and for small external forcing amplitude $\tilde{B}$) the vibration type of regular motion is favored whilst for larger $\tilde{\alpha}$ the rotation one is preferred.

Acknowledgments

We would like to acknowledge fruitful discussions with Dr. W. Przystupa in the early stages of this paper. Authors, Grzegorz Litak, Kazimierz Szabelski and Jerzy Warmiński, were partially supported by State Committee for Scientific Research (KBN) Grant No. 808/T07/96/11. Grzegorz Spuz-Szpos would like to thank DAEWOO Motor Poland for the financial support which led to the opportunity to present part of the results in ENS-Lyon.

References

Baker, G. L. & Gollub, J. P. [1990] *Chaotic Dynamics, An Introduction* (Cambridge University Press, Cambridge).

Guckenheimer, J. & Holmes, P. [1983] *Nonlinear Oscillations, Dynamical Systems, and Bifurcations of Vector Fields* (Springer–Verlag, NY).

Litak, G., Przystupa, W., Szabelski, K. & Warmiński, J. [1994] "Chaotic motion of Froude pendulum" *I.F. UMCS Report.*

Litak, G., Warmiński, J. & Spuz-Szpos, G. [1996] "Chaos analysis of the self–excited system with external forcing," *Proc. Vibrations in Physical Systems, XVII Symp.*, Poznań–Blazejewko, May 22–25, 1996, pp. 188–189.

Minorsky, N. [1962] *Nonlinear Oscillations* (van Nostrand, Princeton, NJ).

Moon, F. C. [1987] *Chaotic Vibrations* (John Wiley, NY).

Nayfeh, A. H. & Sanchez, N. E. [1989] "Bifurcations in a forced softening Duffing oscillator," *Int. J. Non-Lin. Mech.* **24**, 483–497.

Salam, F. M. A. [1987] "The Melnikov technique for highly dissipative systems" *SIAM J. Appl. Math.* **47**, 232–243.

Szabelski, K. & Warmiński, J. [1995] "Self-excited system vibrations with parametric and external excitations," *J. Sound Vib.* **187**, 595–607.

Wiggins, S. [1988] *Global Bifurcations and Chaos* (Springer–Verlag, NY).

Wolf, A., Swift, J. B., Swinney, H. L. & Vasano, J. A. [1988] "Determining Lyapunov exponents from a time series," *Physica* **D16**, 285–317.